Estonian Journal of Engineering, 2008, **14**, 3, 232–254 doi: 10.3176/eng.2008.3.04

Simulation of patterns of wakes from high-speed ferries in Tallinn Bay

Tomas Torsvik[a] and Tarmo Soomere[b]

[a] Bergen Centre for Computational Science, UNIFOB, University of Bergen, Thormøhlensgate 55, N-5008 Bergen, Norway; tomas.torsvik@bccs.uib.no
[b] Centre for Nonlinear Studies, Institute of Cybernetics, Tallinn University of Technology, Akadeemia tee 21, 12618 Tallinn, Estonia; soomere@cs.ioc.ee

Received 22 February 2008, in revised form 3 June 2008

Abstract. We analyse spatial patterns and far field properties of the long-wave part of wakes of fast ferries in Tallinn Bay with the use of the Boussinesq-type shallow-water model COULWAVE, forced by realistic ship motions. The calculated heights of ship waves exhibit substantial spatial variability. The largest waves were created when the ship, sailing to Tallinn, entered into super-critical regime when moving over the coastal slope. The maximum wave height eventually reached 3 m, whereas along other sections of the track the wave height was about 1 m. The highest waves hit the area of Pirita Beach that apparently has much larger ship wave loads than the adjacent sections of the Viimsi Peninsula.

Key words: fast ferries, ship wakes, Boussinesq model, wave modelling.

1. INTRODUCTION

Long and high waves from contemporary high-speed ships have become an important component of the local hydrodynamic activity in a number of inland waterways [1], small bays [2] and archipelago areas [3]. Intense high-speed ship traffic adds a new forcing factor into the local marine ecosystem also in certain semi-enclosed sea areas such as Tallinn Bay [4]. Ship waves usually are of modest height, but may have considerable larger periods than wind waves and swell. The ship wave heights typically do not exceed 1 m, but their periods are frequently about 10–15 s [5]. Such wind waves are very rare in the area in question [6]. The difference in periods, combined with the intensity of ship traffic, is the reason why the role of ship waves is impressive in terms of wave energy and power [7], and wave-induced near-bottom velocities [8]. Ship wakes

form up to about 10% of the annual bulk wave energy and as high portion as 18%–35% (27%–54% during the summer season) from the total wave power at the coasts of Tallinn Bay.

While ship wakes in inland waterways and narrow straits can frequently be approximated by analogous model patterns excited by ships, sailing steadily in uniform channels, determination of such patterns and their spatial and temporal variability in semi-open sea areas with complex bathymetry and geometry is a non-trivial problem. Despite major advances in fluid mechanics and computational fluid dynamics, numerical representation of ship wakes has still remained a major challenge [9]. The key problem is to adequately represent the flow near the vessel and in the far field in a single numerical model. The common opinion is that it is still necessary to validate models based on in situ measurements before they can be used for managing wake wash in a particular situation, regardless of what type of numerical model is the most appropriate [10,11].

The classical Kelvin theory of steady wake, which is frequently used for the description of trans- and supercritical vessel wakes even in seminal studies [11], is clearly justified in cases where a ship sails steadily along a straight track over a sea area with a constant depth. In such cases, the major properties of even highly non-linear wave systems can be derived from the basically linear theory [9,12]. Classical wave propagation and transformation effects such as topographic refraction or bottom-induced damping can be calculated with the use of phase-averaged (spectral) wave models [13–15], or dispersive wave models provided the wake parameters are known in the neighbourhood of the track. The relevant results together with semi-empirical relationships based on field measurements usually give good results in such cases for the far field [11]. Corrections reflecting non-linear (e.g. cnoidal [8]) nature of wave fields in shallow water are also straightforward. Several non-linear effects occurring in the transcritical regime (such as generation and interactions of solitons) can be relatively simply described within weakly dispersive shallow-water frameworks represented by the Korteweg–de Vries and Kadomtsev–Petviashvili equations [16].

As the propagation of wakes from fast ferries involves a multitude of features (effectively two-dimensional wave patterns, non-dispersive solitonic effects, propagation of highly non-linear transient wave groups in which components keep their identity to a large extent, and basically linear effects such as wave refraction and diffraction), none of the above models is able to adequately describe the evolution of the ship wave system in realistic conditions.

To a first approximation, the listed features of wakes of high-speed ships can be reproduced with the use of Boussinesq-type shallow water models. Such models have been frequently applied to specific problems of ship wave propagation [17–21] and have generally led to more realistic results than spectral or non-dispersive wave models [10]. They account for both dispersive and non-linear effects in fully two-dimensional cases. They are able to represent nonsteady effects occurring in the transcritical regime (both in channels [22] and in unbounded sea areas [23,24]) and in the case of non-steady ship motion [20,25].

They also reasonably reproduce spatial patterns of wave crests and key features of wave-wave interactions in areas with complex bathymetry and geometry [17,25]. The overall progress in computational facilities has considerably increased the knowledge of the dynamic description of vessel wakes. The wake patterns can be effectively simulated in areas, covering many square kilometres with a resolution of about 10 m that is sufficient for an adequate description of single wave crests.

The existing high-resolution studies of ship wave patterns have been performed for certain simplified model situations [17,20,25,26], in which the bathymetry was homogeneous in the sailing direction. Simulations with changing Froude number [25] and with an asymmetric channel cross-section [26], performed in such conditions, demonstrated that several important properties of ship waves (such as wave height, orientation of wave crests and wave propagation direction) substantially depended on the sailing regime. As a consequence, the wave loads along the coasts of sea areas, hosting high-speed traffic, may vary considerably depending on wave generation conditions along the ship lane. Such a variation becomes evident from field measurements of the ship wave activity in Tallinn Bay where average wave properties vary more than 20% along a short coastal section (with a length of about 0.5 km) of the eastern coast of the bay located slightly to the north of the border of the computational domain [5,7].

The hydrodynamic loads, created by high-speed vessels, are typically short-time impulses, which are frequently close to or exceeding the damaging levels [2,3,27,28]. Therefore, it is important to adequately estimate the potential variations of wave loads along the ship lane and the locations in which maximum wave loads may occur.

The purpose of the current paper is to establish the magnitude of this variation and the potential location of the largest wave loads in Tallinn Bay. For that purpose we simulate the geometry of patterns of waves, excited by a model ship, matching the sailing track and speed of a realistic, basically randomly chosen, fast ferry – SuperSeaCat on 7 October 2007. The emphasis is on spatial variability of the height of the wake waves in the neighbourhood of the track and on related potential differences in wave loads for different coastal sections.

2. THE NUMERICAL MODEL

Numerical simulations have been executed using a modified version of the COULWAVE model [29]. This model is developed to simulate the evolution of fully non-linear (wave amplitude to water depth ratio of up to $a/h \cong 1$) long waves over a variable bathymetry [30,31]. The model is based on a set of Boussinesq type equations, which have been shown to reproduce the correct dispersion properties for waves as short as $kh \cong \pi$, where k is the wave number. Sponge layers are used at open boundaries to damp out waves, exiting the computational domain. Land cells are declared to be elevated 1 m above the mean water level. Wetting and drying in the coastal zone is enabled by extending

the water level artificially also over the land cells [31]. The reference test cases were run without including any explicit term for wave dissipation, but tests were also run where bottom friction was included to prevent blow up of noise on the grid scale. Other features, available in the model, such as wave breaking and the use of multiple vertical layers, have not been used in our studies. A predictor–corrector scheme is applied to march forward in time, and finite differences are used to approximate the spatial derivatives.

The COULWAVE model has been modified to include wave generation due to a disturbance in the ambient pressure at the free surface. We represent the ship by a moving pressure patch, with centre point at $(x_0(t), y_0(t))$, defined by

$$p(\tilde{x}, \tilde{y}, t) = p_a f(\tilde{x}, t) q(\tilde{y}, t), \tag{1}$$

$$f(\tilde{x}, t) = \begin{cases} \cos^2\left[\dfrac{\pi(\tilde{x} - x_0(t))}{2\alpha L}\right], & \alpha L \le |\tilde{x} - x_0(t)| \le L, \\ 1, & |\tilde{x} - x_0(t)| \le \alpha L, \end{cases} \tag{2}$$

$$q(\tilde{y}, t) = \begin{cases} \cos^2\left[\dfrac{\pi(\tilde{y} - y_0(t))}{2\beta R}\right], & \beta R \le |\tilde{y} - y_0(t)| \le R, \\ 1, & |\tilde{y} - y_0(t)| \le \beta R, \end{cases} \tag{3}$$

on the rectangle $-L \le \tilde{x} - x_0(t) \le L$, $-R \le \tilde{y} - y_0(t) \le R$, and zero outside this region. Values used for the pressure disturbance are $p_a = 1.0$ atm, $L = 50$ m, $R = 20$ m and $\alpha = \beta = 0.75$. The coordinate system for the pressure patch $(\tilde{x}, \tilde{y})$ is generally rotated by some angle θ relative to the global coordinate system (x, y), so the orientation of the pressure patch is transformed according to

$$\tilde{x} = x\cos\theta - y\sin\theta, \quad \tilde{y} = -x\sin\theta + y\cos\theta. \tag{4}$$

The selected parameters give a pressure patch, which is slightly broader than the actual ship hull, but with similar displacement properties (Table 1).

The bathymetry is constructed from a map with a resolution of 1/2′ (463 m) longitude and 1/4′ (470 m) latitude. Interpolation with cubic splines gives a bathymetry with a resolution of 10×10 m, used in simulations. The extent of the computational domain (Fig. 1) was restricted by available computational resources. Within this region there are different types of coastline, harbour areas near the city centre of Tallinn and at Merivälja, and a sandy beach at Pirita.

Table 1. Dimensions of the high-speed craft SuperSeaCat

Length	Beam	Draught	Displacement	Service Speed
100.30 m	17.10 m	2.60 m	340 t	35 knots

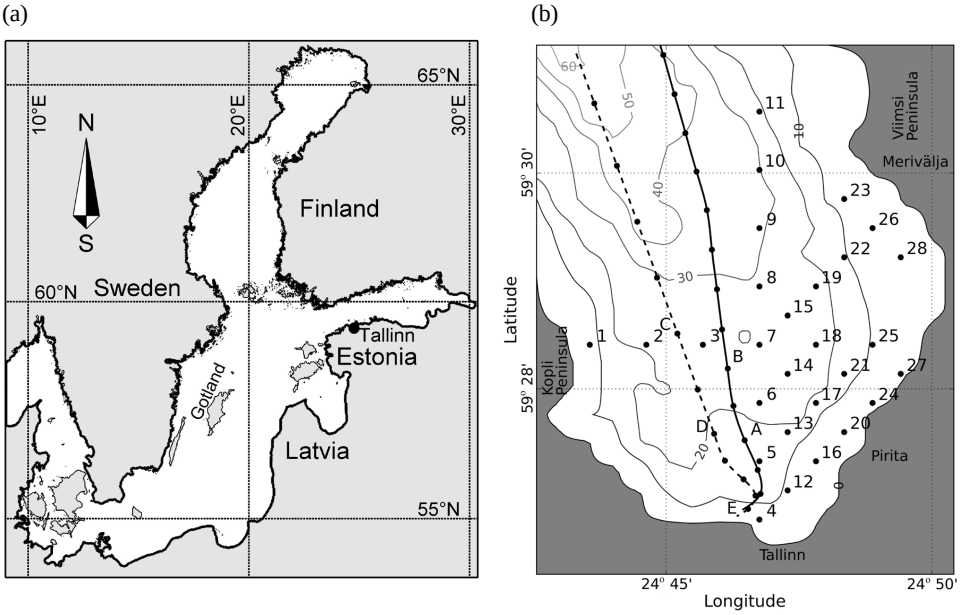

Fig. 1. (a) Location scheme of the Baltic Sea and Tallinn Bay, (b) Map of the inner part of Tallinn Bay. Depth contours are shown at 10 m intervals. The outgoing (solid line) and ingoing (dashed line) ship tracks are marked with black dots indicating points of the ship track recorded by the GPS. Numbered dots show the locations of virtual wave recorders. Capital letters along the tracks indicate the locations of virtual wave recorders for a particular track.

The path, followed by the ship, is based on GPS measurements taken on board of one of the high-speed carriers, servicing the Tallinn–Helsinki route (namely, SuperSeaCat on 7 October 2007), at 1 min intervals (black dots in Fig. 1b). From this data we reconstruct the ship track using interpolation with cubic splines. The velocity profile (Fig. 2), constructed from the interpolation of the ship track, shows a tendency to overshoot at some instances during acceleration.

Simulations have been performed for the inner part of Tallinn Bay, for both the ingoing (southward) and outgoing (northward) ship tracks. The instantaneous vertical displacement of the water surface was recorded every 60 s for the entire domain, and continuously at locations of 28 virtual wave recorders that were more or less uniformly distributed over the computational domain. In addition, virtual wave recorders were located along the ship track at the coordinates of the GPS-recorded positions.

The sensitivity of the model with respect to the grid resolution has been tested by running the simulation for the outgoing ship track with grid steps of $\Delta x = \Delta y = 7.5,\ 10$ and 15 m. The locations of wave gauges No. 12, 15, 24 and 26 matched exactly certain grid points for all three grids, and the comparison between different grid resolutions has been based on results from these gauges. Results for the 15 m resolution was often out of phase with the other two, while results for the 10 and 7.5 m resolution matched fairly well for the leading part of

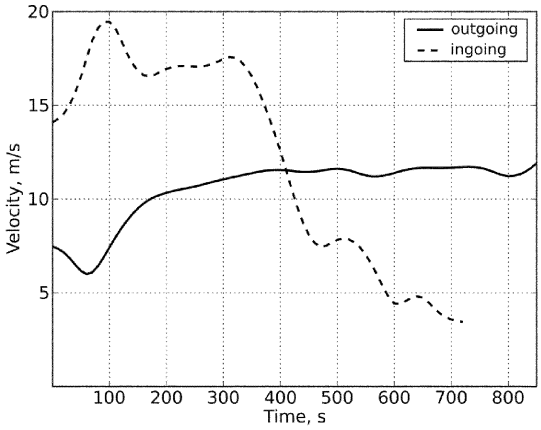

Fig. 2. Estimated ship speed, based on the interpolation of the ship tracks and speeds for outgoing and ingoing ships.

the wave group, particularly for waves with periods of $T > 10$ s. As expected, the details of short-wave components varied greatly for different grid resolutions. However, the average properties of the short-wave fields (wavelengths $< 30-40$ m) matched well in the simulations with 10 and 7.5 m resolution.

3. SHIP TRACKS AND WAVE PATTERNS

The wave-generating properties of a ship in shallow water are characterized by the length Froude number F_L and the depth Froude number F_H, defined by

$$F_L = \frac{U}{\sqrt{gL_W}}, \quad F_H = \frac{U}{\sqrt{gh}} \tag{5}$$

respectively, where U is the speed of the ship, g is the acceleration of gravity, L_W is the length of the ship's waterline, and h is the water depth. The wave-making resistance has a maximum in the so-called hump speed region $0.4 \le F_L \le 0.6$. For a ship with $L_W = 100$ m, the hump speed lies within the range from 12.5 to 18.8 m/s. In shallow water, the water depth also influences the wave-making resistance, the maximum of which occurs near the critical depth Froude number $F_H = 1$. Sailing speeds, corresponding to $0.85 \le F_H \le 1.15$, are frequently called transcritical speeds [9].

For the outgoing track (Fig. 3a), both Froude numbers are below the most dangerous regime: $F_L \cong 0.5$, $F_H \cong 1$. Early in the track the depth Froude number is $F_H \cong 0.7$, which is large enough for shallow water effects to be significant [9]. For the ingoing track (Fig. 3b), both Froude numbers come within the dangerous regime at the same time. Thus one can expect long, large amplitude waves to be generated in this case.

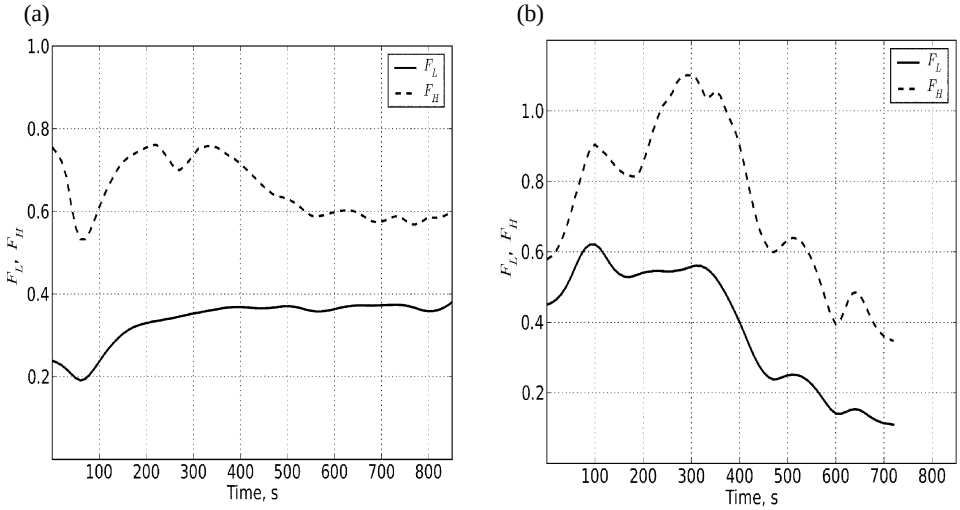

Fig. 3. Depth and length Froude numbers for outgoing (a) and ingoing (b) ship tracks.

We have simulated the wave generation and evolution for ferries on both ingoing and outgoing tracks from Tallinn. A selection of wave patterns is shown in Fig. 4. As could be expected, the wave impact in the inner part of Tallinn Bay differs significantly in these two cases. Waves from ingoing ships mainly impact the southern regions of the coast (Fig. 4d), whereas waves generated by outgoing ships (Fig. 4b) mainly impact the coast near Merivälja. In reality, the wave impact on the eastern coast should be larger than is shown for the incoming case, but these waves are underestimated in the current study due to the limitations of the computational domain.

A striking feature of the outgoing case is the asymmetry of the wake waves, which is particularly pronounced in the early part of the simulation (Fig. 4a). This becomes more apparent if we compare wave gauges 3 and 7 (Fig. 5). There are no evident topographical features that can create this asymmetry. Most probably, the manoeuvres at the start of the track have caused the wave focusing on the left-hand side of the track. In principle, it is not excluded that this asymmetry is a numerical artefact created by the effects related to the orientation of the pressure patch that simulates the ship motion. The patch is symmetrical as long as it is oriented along the north-south or east-west axis. The symmetry is lost when the patch is tilted with respect to these axes and is interpolated on a fairly coarse grid in the scale of the ship's hull.

Figure 5 also reveals the dispersive properties of waves with intermediate wave lengths. While the initial wave group is fairly compact (Fig. 5c), the wave group becomes broader further away from the ship track (Fig. 5b). Only a small portion of the wave energy reaches the shallow area around the gauge 1 (Fig. 5a). The reason is the finite length from the wave train that passes northwards of the location of the wave gauge 1. Thus, this wave gauge is implicitly sheltered from waves generated by outgoing ships.

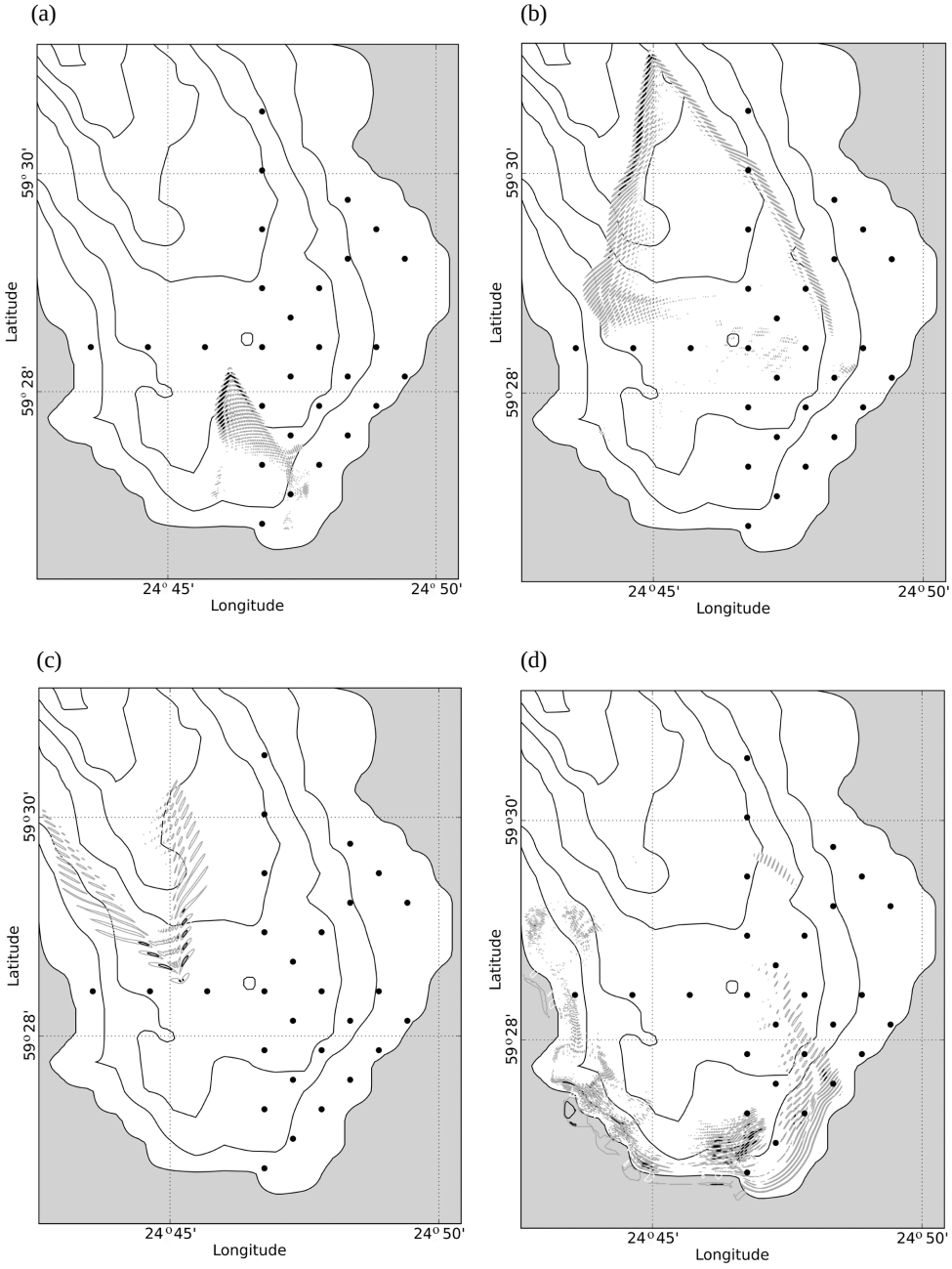

Fig. 4. Spatial wave patterns: (a) outgoing ship, $T = 300$ s; (b) outgoing ship, $T = 780$ s; (c) ingoing ship, $T = 300$ s; (d) ingoing ship, $T = 660$ s. Depth contours (bold) are shown at 10 m intervals. Contour lines in shaded areas are drawn for surface elevation above the mean sea level only, with contour lines at 0.25 and 0.75 m.

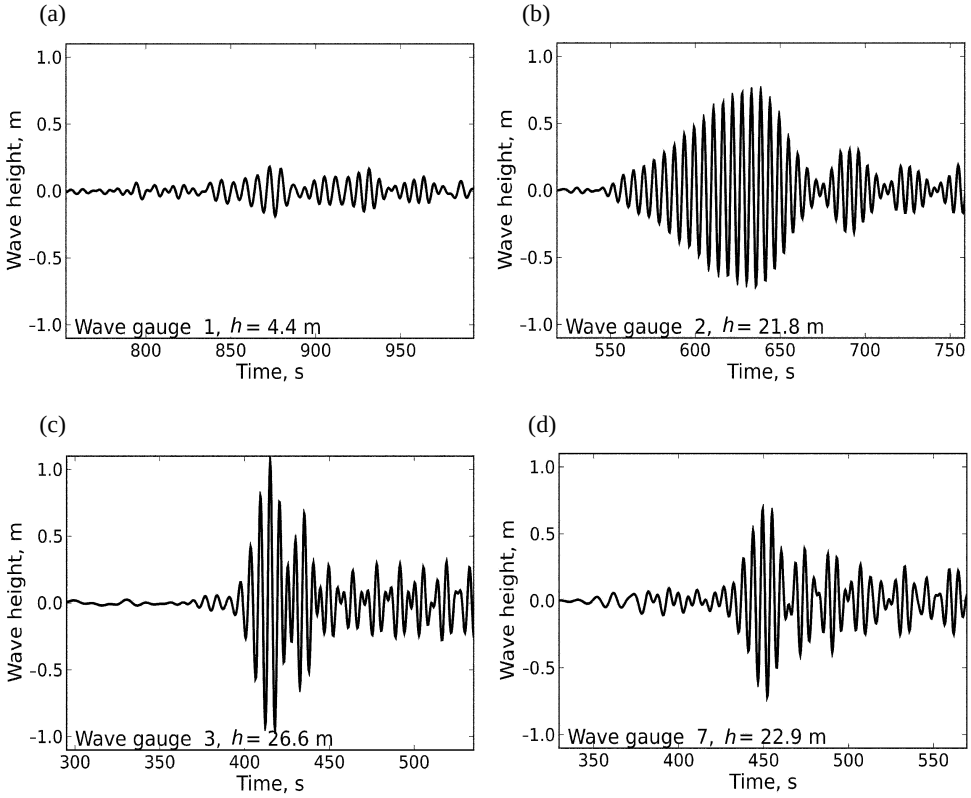

Fig. 5. Surface elevation time series at selected virtual wave gauges, located across Tallinn Bay for the outgoing track. The numbers of the gauges in Fig. 1 and water depth are indicated on the panels.

An extremely large wave can be seen immediately following the outgoing ship along a certain section of the sailing track (Fig. 6a). This is atypical for the wave recordings along the track, which are mostly similar to the record shown in Fig. 6b. Although the pressure patch that is used to generate the waves does not reproduce the details of the flow around a ship hull, it is nevertheless remarkable that such a wave occurs in our results. This wave appears while the ship is accelerating and the depth Froude number is about 0.7. Earlier studies have shown that large waves may be generated during acceleration for $F_H \cong 1$ [25,32], but in these studies little attention has been paid to waves generated during acceleration in the subcritical range $F_H < 1$. The large amplitude wave seems to be a highly localized and transient phenomenon because it can be identified neither in nearby wave gauges 5 and 6 (Fig. 1), nor in any of the wave gauges further along the track.

Visual inspection of Figs. 4a and 4c suggests that the longest waves, generated for the ingoing track, have significantly larger periods than the waves generated for the outgoing track. This becomes clearer if we compare the properties of the wave field across the bay for outgoing (Fig. 5) and ingoing tracks (Fig. 7).

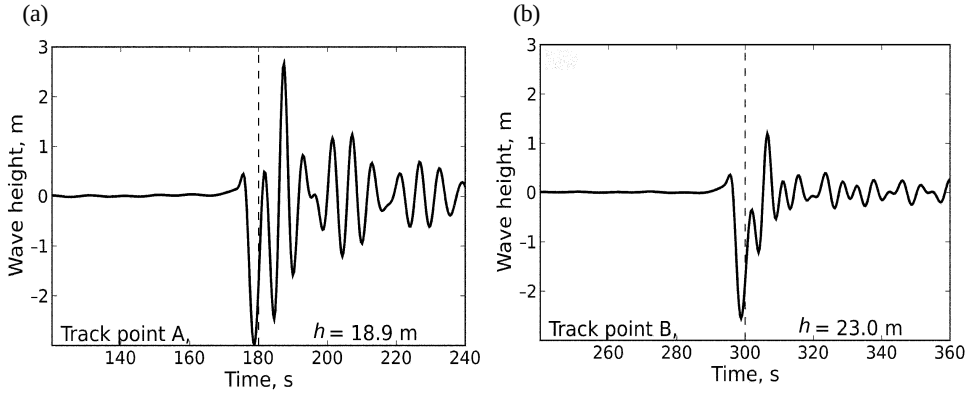

Fig. 6. Surface elevation time series at virtual wave gauges at selected points along the outgoing ship track: (a) track point A, $T = 180$ s; (b) track point B, $T = 300$ s. Time T (indicated by vertical dashed lines) shows when the ship passed the location of the wave gauge. The location of the gauge in Fig. 1 and water depth are indicated on the panels.

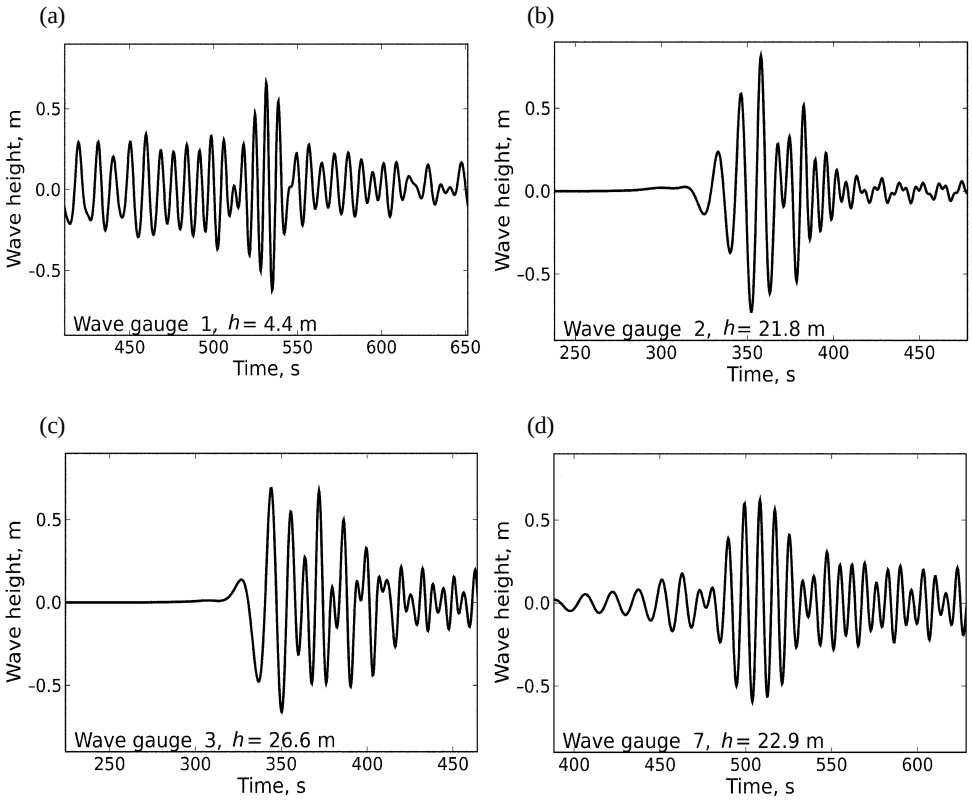

Fig. 7. Surface elevation time series at selected virtual wave gauges, located across Tallinn Bay for the ingoing track. The number of the gauge in Fig. 1 and water depth are indicated on the panels.

Based on records from wave gauges 3 and 7, we estimate the wave period for the leading wave group in the ship wake to be $T \cong 5.5\,\mathrm{s}$ for the outgoing and $T \cong 9\,\mathrm{s}$ for the ingoing track. These results match fairly well the values given in the Appendix for all the wave gauges. In general, this difference in periods simply reflects the difference of typical sailing speed along ingoing and outgoing tracks (see Section 5).

It is also interesting to note that the entire wave pattern for the ingoing track is more symmetric than for the outgoing track. The wave amplitudes at wave gauges 2, 3 and 7 differ insignificantly for the ingoing track (Fig. 7). This feature can be interpreted as showing that the orientation of the pressure patch is not responsible for the asymmetric features found above for the outgoing track. Given the difference in wave periods for the ingoing and outgoing tracks, grid size effects may be more influential in the latter than in the former case. However, this is not supported by the grid sensitivity test (Section 2), which shows that the general features of the ship wakes are consistent between the $\Delta x = 7.5$ m and $\Delta x = 10$ m simulations.

The ingoing ship moves at supercritical depth Froude numbers $F_H > 1$, starting from 250 s for about 120 s (Fig. 3b). The maximum value of $F_H \cong 1.1$ was reached at 297 s. Figure 4a shows the spatial wave pattern, generated for supercritical depth Froude numbers. The wave gauges along the ingoing track (Fig. 8) do not show any large waves in the wake for T = 300 and 360 s, but there is a slight increase in the amplitude of the bow wave. From 350 to 450 s the ship went through a rapid deceleration and started to interact with waves from its own wake. The waves with the largest amplitudes occur near the ship after T = 420 s (Fig. 8b). Thereafter the ship is preceded by a train of long waves, the leading wave of which originates from the supercritical bow wave. When the ship is nearly in the harbour, at T = 660 s (Fig. 8c), it is preceded by approximately 10 waves, the first of which arrives about 2 minutes before the ship. The recordings at T = 420 and 660 s (Figs. 8b and 8c) contain a gradually lengthening depression area around the ship. Such areas are characteristic for transcritical ship wakes [9].

The discussed features correspond well with what has been described elsewhere [25,32]. Therefore, the results of previous studies that used idealized test cases match well with the main properties of ship wakes over realistic bathymetry and ship motion.

Figure 4d gives insight to the potential impact of ship waves at the shore. Its important feature is the very inhomogeneous spatial distribution of the largest wave heights. For instance, a region of the coast just east of the 24°45′ mark receives almost no large amplitude waves, whereas high waves are present on parts of the coast line at both its sides. This indicates that the bathymetry may considerably shape the wave pattern and may create wave focusing and shadowed areas in certain regions.

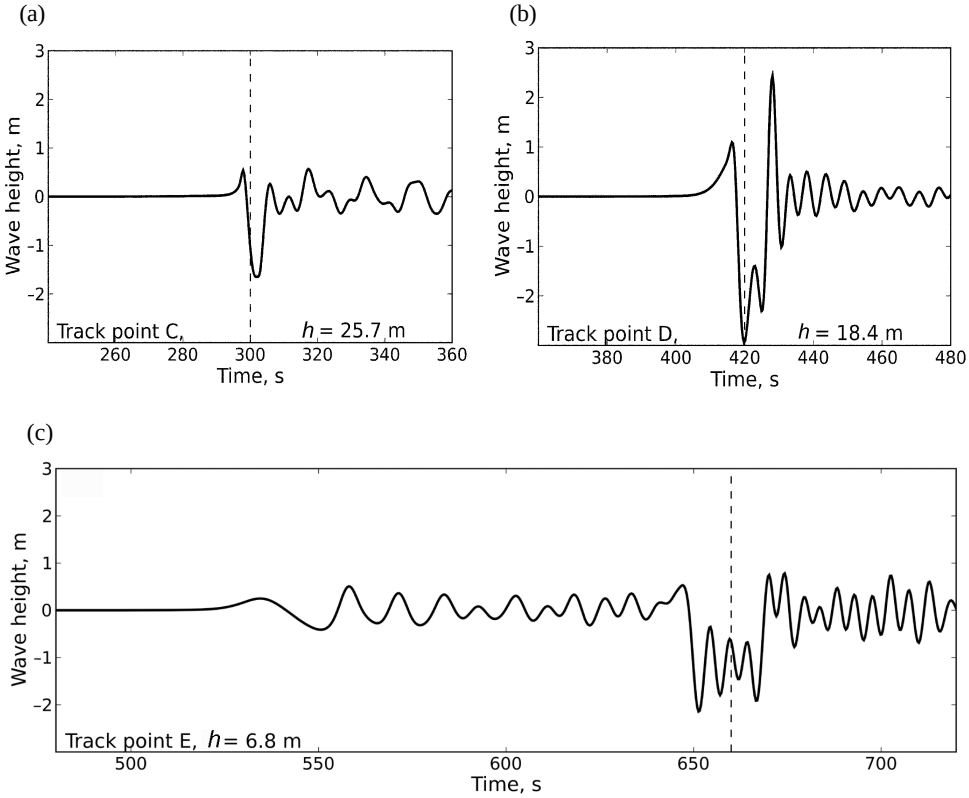

Fig. 8. Surface elevation time series at virtual wave gauges at selected points along the ingoing ship track: (a) track point C, $T = 300$ s; (b) track point D, $T = 420$ s; (c) track point E, $T = 660$ s. Other notations are the same as in Fig. 6.

4. WAVES AT MERIVÄLJA AND AT PIRITA BEACH

In this section we focus on the wave properties near Merivälja and Pirita Beach. The Merivälja area (as well as a section of the coast of Viimsi Peninsula, located more northward from the computational domain) receives the main wave impact from outgoing ships, whereas ingoing ships produce the main wave impact at Pirita Beach. It is convenient to track the changes of the wake along its propagation by taking the wave signal at wave gauge 7 as the origin. The propagation of the ship wakes for the ingoing and outgoing tracks are reflected in numerical wave gauges located along straight lines to wave gauges 20 and 26, respectively. The resulting lines are nearly perpendicular to the respective sections of the coastlines.

Several factors may influence the evolution of waves from their point of origin until they reach the shore, such as the shape of the initial wave signal, the distance travelled, or the particular shape of the topography. The depth profiles along the lines in question are shown in Fig. 9. The distance from wave gauge 7

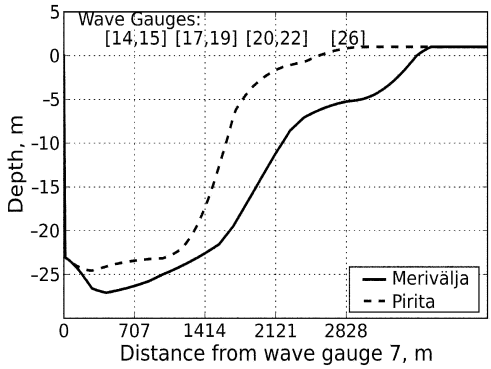

Fig. 9. Variation of water depth along straight lines from wave gauge 7 to Merivälja and Pirita Beach.

to Pirita is somewhat shorter than the distance to Merivälja. The most important difference of the shape of the profiles is that there is a shallow region with a depth less than 2 m extending some distance offshore from Pirita, whereas the offshore slope in the bathymetry at Merivälja is fairly steep at depths down to 4 m, but forms a terrace at depths from 4 to 6 m [33].

Figure 10 shows results from wave recorders along lines from the wave gauge 7 towards Merivälja and Pirita Beach. The maximum wave amplitudes for the in- and outgoing tracks are nearly equal, but the wave periods for the outgoing ship are much smaller than for the ingoing one. This difference is a major source for the much faster wave propagation towards Pirita for the ingoing case compared to the speed of propagation towards Merivälja for the outgoing case. The relatively short-period waves from the outgoing ship traverse the distance from wave gauge 7 to wave gauge 19 (1414 m) in about 300 s (Fig. 10c), whereas longer waves from the ingoing ship traverse the same distance to wave gauge 17 in about 100 s (Fig. 10d). The orientation of the wave group relative to the locations of the wave gauges makes it difficult to extract exact wave speeds out of these data. There is no topographical feature to explain this difference, so the difference in wave speed must be related to the combination of the difference in wave periods and internal structure for the ingoing and outgoing cases.

The wave amplitudes diminish slightly as the waves progress away from the ship track. The rate of decline seems to be nearly equal for the long-period and short-period waves. This can be seen from the wave amplitudes in wave gauges 19 (Fig. 10c) and 17 (Fig. 10d), and is confirmed by the values given in the Appendix.

The wave amplitudes continue to diminish as the waves propagate towards Merivälja. The wave gauge near the coast (Fig. 10e) shows that the waves are not amplified significantly by wave shoaling. This is an expected feature, reflecting the shortness of ship waves for the outgoing track (cf. Appendix).

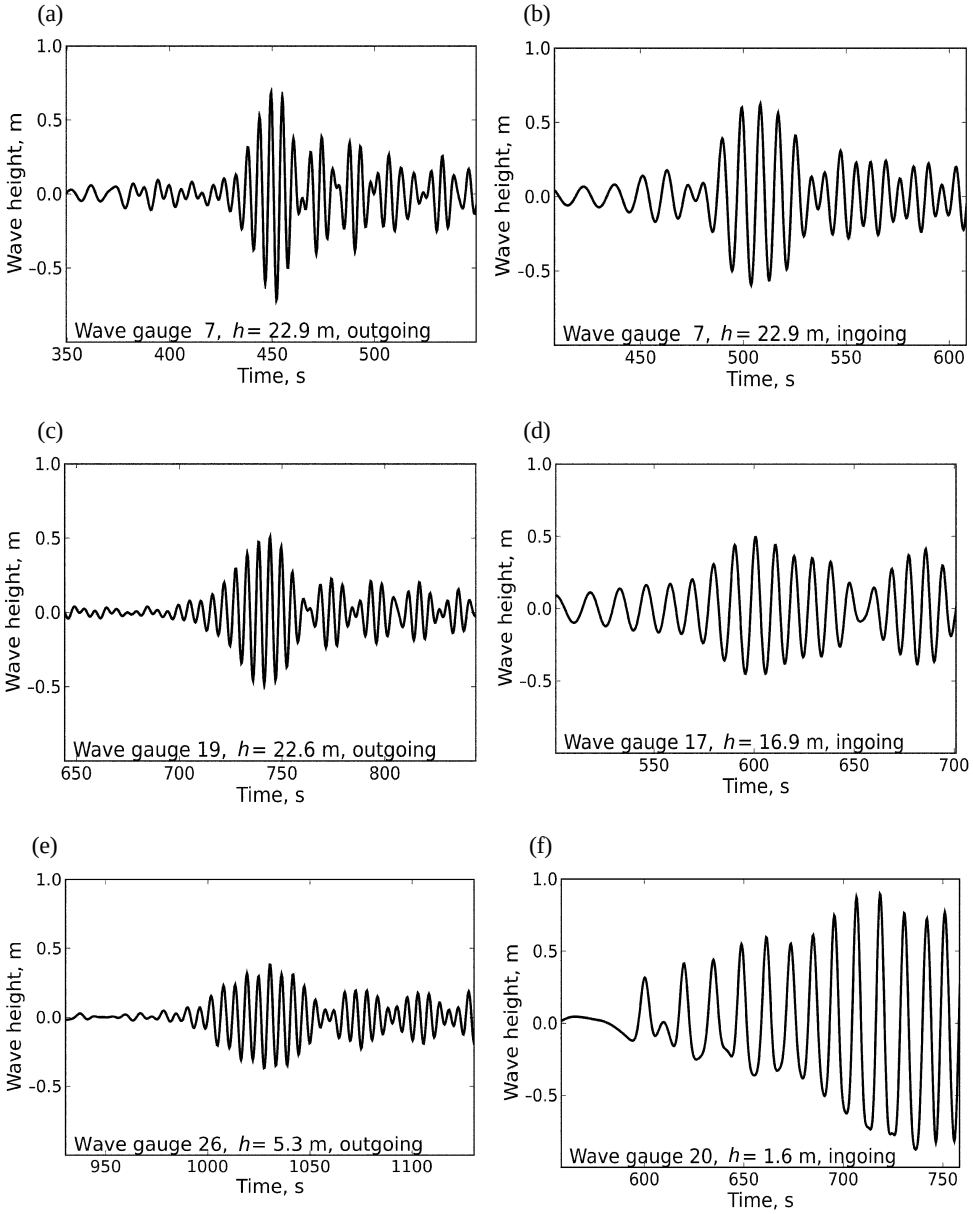

Fig. 10. Surface elevation time series in waves formed by an outgoing ship and propagating towards Merivälja (a, c, e); waves formed by an ingoing ship and propagating towards Pirita Beach (b, d, f).

There is a significant spatial variability in the wave properties along the coastline of Merivälja. The records of wave gauges 23 and 26 show a distinct ship wave signal, with a maximum wave amplitude of about 40 cm. Almost no

wave signal is present at wave gauge 28, where wave amplitudes do not exceed 4 cm. This feature apparently reflects the limited extension of the ship-induced wave fan (cf. Section 3).

Longer waves, created by incoming ships and approaching Pirita Beach, may be amplified significantly due to the wave shoaling process. The waves recorded at wave gauge 20 (Fig. 10f) are extremely large, close to the breaking stage, considering the water depth of $h = 1.6$ m at this location. Their height may be to some extent overestimated as the bottom friction and wave breaking were not included in the model. Figure 4d suggests that effects of wave focusing at this location may contribute to the amplification due to wave shoaling to some extent. Regardless of whether or not the waves are exactly represented, it is clear that the wave impact on Pirita Beach may be significantly larger than for other parts of the bay. This is related to the fact that the ships may operate at near-critical depth Froude numbers when approaching Tallinn Harbour. The waves generated at this time mainly impact Pirita Beach.

5. LIMITATIONS OF INVISCID SIMULATIONS AND THE LINEAR THEORY

The above discussion of wave generation and propagation in relatively deep areas is based on the results from the runs in which the bottom friction was neglected. Doing so is clearly justified for most of Tallinn Bay. The situation is different in shallow coastal areas where the combination of diffractive effects with partial wave reflection and numerical noise may considerably affect the quality of the results. For example, the reference simulation for the ingoing ship track crashed after 920 s. As the model was run without bottom friction and wave breaking, wave energy dissipation rate in the shoaling process was obviously underestimated. This led to the formation of strong grid scale noise in wave packets reflected back from the coast. To partially overcome the problem, a series of test runs was performed with bottom friction for the ingoing track case. Bottom friction was modelled as

$$R_f = \frac{r}{h+\eta} u\,|u|, \tag{6}$$

where u is water velocity, η is the surface displacement and r is the bottom friction coefficient. Several runs were needed to calibrate the bottom friction and to obtain realistic results in the near-coastal area. Lynett et al. [31] found an optimum value of $r = 0.005$ in their study of wave runup. For the case in question, however, this choice did not lead to stable simulations. We ran the simulation for the bottom friction parameter ranging from $r = 0.01$ to 0.05. The simulation ran without crashing only in the latter case, which we adopted as our best choice of the bottom friction parameter as it is the smallest value giving a

stable run. Notice that the value $r = 0.05$ may be too large to accurately model the shoaling and runup processes in the immediate nearshore.

A comparison of the wave field at wave gauge 20 for the reference simulation and for the case when bottom friction was included is presented in Fig. 11. As expected, the wave amplitudes in the run with bottom friction are significantly reduced compared with the reference run. The entire wave packet in the former case resembles the factually measured ship wave signal. The maximum wave amplitude (about 40 cm) in this run is very reasonable in the light of the existing data from Tallinn Bay. The arrival time and wave period are coinciding fairly well in the two runs. This feature suggests that the reference simulation adequately represents the ship wave signal up to a reasonable distance from the coast. It is, however, not possible to say which of the two results bears the closest resemblance to the real wave conditions in nearshore without comparing to data from field measurements. Such data have been reported for several sections of the coast of Tallinn Bay [5]. Unfortunately, no relevant data existed for Pirita Beach at the time of writing, but this will hopefully be remedied by a measurement program for the Tallinn Bay area that is planned for the next few years.

The results, presented above, were obtained using the highly non-linear COULWAVE model. In this context it is of interest to examine the contribution of the non-linear terms, specifically, where and how these effects are manifested, and to what extent the results coincide with the linear theory. For this purpose we have also made simulations with COULWAVE, where we have turned off all non-linear terms, governing wave propagation, but retained the purely dispersive terms.

A comparison of the results, obtained from the linear and non-linear simulations, demonstrates that the wave profiles along the track are virtually indistinguishable even at $T = 300$ s, when $F_H > 1$ (Fig. 12a). Even for the long period precursor waves there is a fairly good match between the linear and non-linear simulations for the leading wave group (Fig. 12b). The records at wave gauges 1 and 16 (Figs. 12c and 12d, respectively) indicate that the non-linear

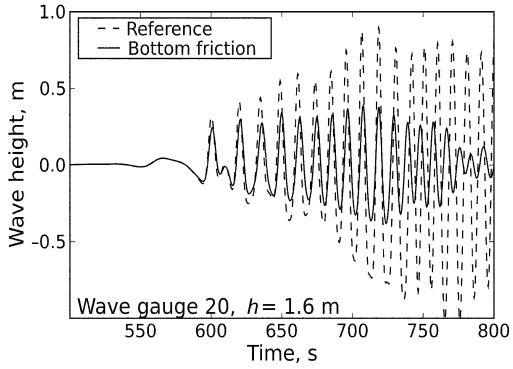

Fig. 11. Surface elevation time series at virtual wave gauge 20, with (solid line) and without (dashed line) bottom friction.

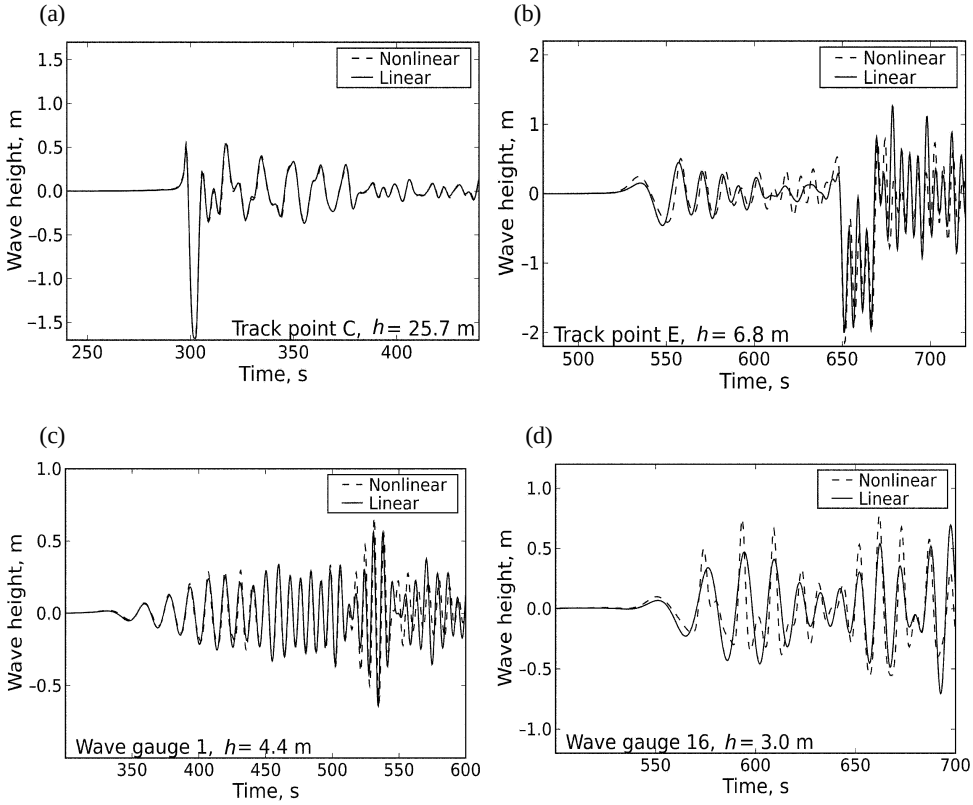

Fig. 12. Surface elevation time series at selected virtual wave gauges across Tallinn Bay and along the ingoing ship track in non-linear and linear simulations: (a) track point C, $T = 300$ s; (b) track point E, $T = 660$ s; (c) wave gauge 1; (d) wave gauge 16. The numbers of virtual gauges in Fig. 1 and water depth are indicated on the panels.

terms do influence the wave amplitude during shoaling. This impact increases, as expected, with increasing wave amplitudes. The non-linear effects also seem to increase with increasing wave periods. This conclusion is supported by simulations of the outgoing track. Waves excited by the outgoing ship had generally smaller wave periods and the difference between the results of linear and non-linear simulations were clearly smaller than for the ingoing track.

Wake wave periods generally depend on the ship speed and the local depth. The relevant estimates for deep water waves are presented in classical texts and overviews [9,12]. A simple estimate for the wave period in a steady Kelvin wake (Fig. 13) can be obtained from the following relation between the angular frequency ω of the largest waves in the wave group and the ship speed:

$$\omega = kU\cos\theta, \tag{7}$$

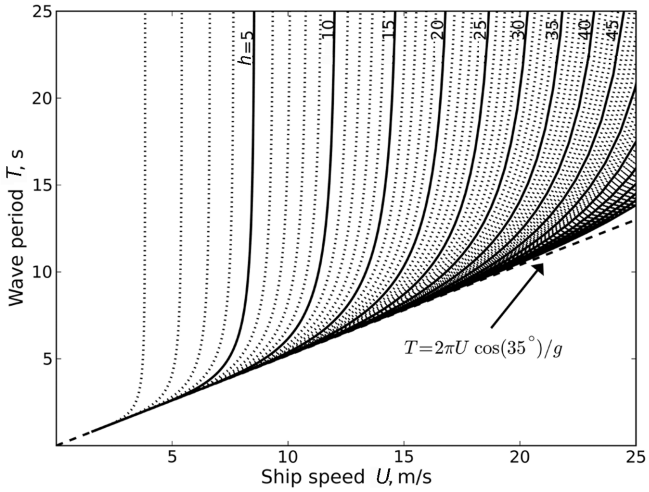

Fig. 13. Speed dependence of wave periods for the Kelvin ship wake at different depths *h*. Dashed line indicates wave period in deep water.

where $\theta \cong 35°$ is characteristic for the Kelvin wake in deep water and increases with the decrease of the water depth. The wave number can be determined from the linear dispersion relation for water over finite depth

$$\omega^2 = gk \tanh(kh). \tag{8}$$

Notice that the sudden steepening of the lines at different depths in the upper part of Fig. 13 does not indicate a dramatic increase in the wave period, but rather that the assumption of the existence of steady, linear Kelvin wake no longer applies.

Although a steady Kelvin wake does not necessarily exist for fast ferries, sailing at transcritical speeds in Tallinn Bay, the relevant theory is still useful for obtaining a rough estimate of the wave period in subcritical regime. For $U = 12$ m/s and $h > 15$ m, the theory predicts wave periods of slightly more than 5 s. This is within the range, given by most of the wave gauges for the outgoing track (Table 2). The sailing speed along the ingoing track varies largely. The rough estimate of the speed until $T = 350$ s is $U = 17$ m/s. At this speed and for $h > 40$ m we get wave periods of slightly less than 10 s. This matches well the properties of leading waves at several gauges for the ingoing track (Table 2). Some wave gauges show considerably longer wave periods, such as wave gauge 3, which is located close to the ship track. Moreover, wave gauges 4, 13 and 16 show evidence of long precursor waves (Fig. 8c). We may therefore conclude that the presented rough estimate satisfactorily represents the properties of a large part of ship wakes, but fails to reproduce properties of specific waves, excited in transcritical regime.

6. CONCLUSIONS AND DISCUSSION

The features of the bathymetry of Tallinn Bay and restrictions for the choice of the sailing line allow high-speed ships to sail mostly in subcritical regime. Although the track of the outbound (Tallinn–Helsinki) leg follows the steep underwater slope along the deep trench in the middle of Tallinn Bay, the factual sailing line is located in deep enough area to avoid generation of transcritical wave systems during the acceleration phase.

The track of the inbound leg is located in the deepest part of the depth along the section from the bay entrance down to the latitude of Merivälja (Fig. 1). The water depth, however, decreases considerably when the ships cross this line. As the incoming leg stretches along the underwater slope, it is highly probable that the vessels, operated in a standard sailing routine, will come close to the critical speed or even enter the supercritical regime. Our observations show that the time interval, during which the ship sails in transcritical regime, is a few minutes. Consequently, the lengths of the wave crests of the near-critical wake are of the order of 1–2 km. Such waves are effectively non-diffractive and may remain compact for a long time [9].

The exact location of the generation of such a wake and the section of affected coast depends on the particular sailing line and ship speed. The right-hand part of the transcritical wake apparently hits the coast of the Kopli Peninsula northwards from the computational domain. The highest section of the left-hand part of the wake usually reaches Pirita Beach. As the coast of the Viimsi Peninsula northwards from Pirita Beach is usually affected by clearly subcritical wakes from inbound ships, the factual ship wave loads at Pirita may be quite large. Therefore, it is likely that Pirita Beach is actually exposed to more ship wave energy than other parts of the Viimsi Peninsula, although simple spatial interpolation of ship wave activity, based on several wave measurement sites, may suggest an opposite view [7]. This feature may play a certain role in the evolution of Pirita Beach [33] which is generally thought to be exposed to less ship wave energy than the Viimsi Peninsula [34].

The central conclusion from our simulations is that wave loads along the coasts of Tallinn Bay evidently vary largely. High, long-crested, practically non-diffractive and only weakly dispersive wave groups are apparently generated along a few sections of the tracks. This feature is further enhanced by the unfavourable dimensions of some ships. For example, the design speed of SuperSeaCat corresponds to the length Froude number about 0.4. For outbound ferries, the highest waves usually occur at the end phase of the ship's acceleration. The orientation of the track is such that these groups usually only reach the coast of the Viimsi Peninsula northwards from Merivälja. The coast there is well protected by rocky shallow areas and the influence of ship waves on the nearshore is very limited [7]. There is no such protection for the southern part of the Aegna Island that is known to be frequently hit by large waves [5,7]. Inbound vessels may create very high waves in some sections of the western coast of Tallinn Bay.

The discussed features offer a new explanation as to why the properties of different wakes have a large scatter at all measurement sites [5,7,15]. This feature has frequently been attributed to the overall sensitivity of wave generation conditions even on secondary parameters such as the load and trim of the ship [15]. It may, however, stem from the fact that the generation of high waves is intrinsically restricted to a few sections of the ship track. Owing to the asymmetry of the wave generation for accelerating and decelerating ships [25], these sections generally are different for in- and outbound ships even if they use the same sailing line. This property offers a way to further reduce the damaging potential of ship wakes by a making smart operational choices in the sea area where the highest waves are generated.

ACKNOWLEDGEMENTS

This study has been supported by the Estonian Science Foundation (grants Nos. 7000 and 7413) and by the Centre for Nonlinear Studies (CENS) at the Institute of Cybernetics, Tallinn University of Technology. A large part of the work was done when one of the authors (TT) was visiting the Centre for Nonlinear Studies in the framework of the Marie Curie Transfer of Knowledge project CENS-CMA (MC-TK-013909). Friendly and constructive remarks and suggestions of Kevin Parnell and an anonymous referee are gratefully acknowledged.

REFERENCES

1. Bourne, J. Louisiana's vanishing wetlands: Going, going... *Science*, 2000, **289**, 1860–1863.
2. Schoellhamer, D. H. Anthropogenic sediment resuspension mechanisms in a shallow microtidal estuary. *Estuar. Coast. Shelf Sci.*, 1996, **43**, 533–548.
3. Lindholm, T., Svartström, M., Spoof, L. and Meriluoto, J. Effects of ship traffic on archipelago waters off the Långnäs harbour in Åland, SW Finland. *Hydrobiologia*, 2001, **444**, 217–225.
4. Soomere, T. Fast ferry traffic as a qualitatively new forcing factor of environmental processes in non-tidal sea areas: a case study in Tallinn Bay, Baltic Sea. *Environ. Fluid Mech.*, 2005, **5**, 293–323.
5. Soomere, T. and Rannat, K. An experimental study of wind waves and ship wakes in Tallinn Bay. *Proc. Estonian Acad. Sci. Eng.*, 2003, **9**, 157–184.
6. Soomere, T. Wind wave statistics in Tallinn Bay. *Boreal Environ. Res.*, 2005, **10**, 103–118.
7. Soomere, T., Elken, J., Kask, J., Keevallik, S., Kõuts, T., Metsaveer, J. and Peterson, P. Fast ferries as a new key forcing factor in Tallinn Bay. *Proc. Estonian Acad. Sci. Eng.*, 2003, **9**, 220–242.
8. Soomere, T., Põder, R., Rannat, K. and Kask, A. Profiles of waves from high-speed ferries in the coastal area. *Proc. Estonian Acad. Sci. Eng.*, 2005, **11**, 245–260.
9. Soomere, T. Nonlinear components of ship wake waves. *Appl. Mech. Rev.*, 2007, **60**, 120–138.
10. *Guidelines for Managing Wake Wash from High-speed Vessels*. Report of the Working Group 41 of the Maritime Navigation Commission. International Navigation Association (PIANC), Brussels, 2003.
11. Parnell, K. E. and Kofoed-Hansen, H. Wakes from large high-speed ferries in confined coastal waters: Management approaches with examples from New Zealand and Denmark. *Coast. Manage.*, 2001, **29**, 217–237.

12. Sorensen, R. M. Ship-generated waves. *Adv. Hydrosci.*, 1973, **9**, 49–83.
13. Kirk McClure Morton. *Investigation of High Speed Craft on Routes Near to Land or Enclosed Estuaries*. Research Report JR226, Maritime and Coastguard Agency, UK, 1998.
14. Kofoed-Hansen, H. *Technical Investigation of Wake Wash from Fast Ferries*. Report No. 96-5012, Danish Hydraulic Institute, Copenhagen, 1996.
15. Kofoed-Hansen, H. and Mikkelsen, A. C. Wake wave from fast ferries in Denmark. In *Proc. 4th International Conference of Fast Sea Transportation FAST'97*. Sydney, 1997. Baird Publications, Hong Kong, Sydney, 1997, vol. 1, 471–478.
16. Lee, S. J. and Grimshaw, R. H. J. Upstream-advancing waves generated by threedimensional moving disturbances. *Phys. Fluids A*, 1990, **2**, 194–201.
17. Jiang, T. *Ship Waves in Shallow Water*. Fortschritt-Berichte VDI, Reihe 12, No. 466, VDI Verlag, Düsseldorf, 2001.
18. Chen, X. N. and Sharma, S. D. A slender ship moving at a near-critical speed in a shallow channel. *J. Fluid Mech.*, 1995, **291**, 263–285.
19. Jiang, T. Investigation of waves generated by ships in shallow water. In *Proc. 22nd Symposium on Naval Hydrodynamics*. Washington D.C., 1998. National Academy Press, Washington D.C., 1999, 601–612.
20. Jiang, T., Henn, R. and Sharma, S. D. Wash waves generated by ships moving on fairways of varying topography. In *Proc. 24th Symposium on Naval Hydrodynamics*. Fukuoka, Japan, 2002. National Academy Press, Washington D.C., 2003, 441–457 (web only: www.nap-edu).
21. Kofoed-Hansen, H., Jensen, T., Sørensen, O. R. and Fuchs, J. Wake wash risk assessment of high-speed ferry routes – a case study and suggestions for model improvements. In *Proc. International Conference on Hydrodynamics of High Speed Craft, Wake Wash and Motion Control*. London, 2000. The Royal Institute of Naval Architects, 2000.
22. Katsis, C. and Akylas, T. R. On the excitation of long nonlinear water waves by a moving pressure distribution. Part 2. Three-dimensional effects. *J. Fluid Mech.*, 1987, **177**, 49–65.
23. Li, Y. and Sclavounos, P. D. Three-dimensional nonlinear solitary waves in shallow water generated by an advancing disturbance. *J. Fluid Mech.*, 2002, **470**, 383–410.
24. Choi, H. S., Bai, K. J., Kim, J. W., Kim, Y. H. and Cho, H. Nonlinear free surface waves due to a ship moving near the critical speed of shallow water. In *Proc. 18th Symposium on Naval Hydrodynamics*. Ann Arbor, 1990. National Academy Press, Washington D.C., 1990, 173–190.
25. Torsvik, T., Dysthe, K. and Pedersen, G. Influence of variable Froude number on waves generated by ships in shallow water. *Phys. Fluids*, 2006, **18**, Paper 062101.
26. Belibassakis, K. A. A coupled-mode technique for the transformation of ship-generated waves over variable bathymetry regions. *Appl. Ocean Res.*, 2003, **25**, 321–336.
27. Soomere, T. and Kask, J. A specific impact of waves of fast ferries on sediment transport processes of Tallinn Bay. *Proc. Estonian Acad. Sci. Biol. Ecol.*, 2003, **52**, 319–331.
28. Erm, A. and Soomere, T. Influence of fast ship waves on optical properties of sea water in Tallinn Bay, Baltic Sea. *Proc. Estonian Acad. Sci. Biol. Ecol.*, 2004, **53**, 161–178.
29. Lynett, P. and Liu, P. L.-F. COULWAVE model page: Modeling wave generation, evolution, and interaction with depth-integrated, dispersive wave equations. http://ceprofs.tamu.edu/plynett/COULWAVE/
30. Lynett, P. and Liu, P. L.-F. A numerical study of submarine landslide generated waves and runup. *Proc. Roy. Soc. Lond. A*, 2002, **458**, 2885–2910.
31. Lynett, P., Wu, T.-R. and Liu, P. L.-F. Modeling wave runup with depth-integrated equations. *Coast. Eng.*, 2002, **46**, 89–107.
32. Redekopp, L. G. and You, Z. Passage through resonance for the forced Korteweg-de Vries equation. *Phys. Rev. Lett.*, 1995, **74**, 5158–5161.
33. Soomere, T., Kask, A., Kask, J. and Nerman, R. Transport and distribution of bottom sediments at Pirita Beach. *Estonian J. Earth Sci.*, 2007, **56**, 233–254.
34. Soomere, T., Kask, A. and Kask, J. Pirita rannavööndi keskkonnauuringud ja rannakaitse rajatiste projekteerimise lähteülesanne. Research report. TTÜ Küberneetika Instituut, Tallinn, 2005.

APPENDIX

In order to present a flavour about the spatial variability of the ship wave patterns, wave records and data from all the virtual wave recorders, shown in Fig. 1, are given in Figs. 14 and 15 and in Table 2. Wave periods are approximated only for wave amplitudes larger than 20 cm as the time difference between the highest and the following wave crest.

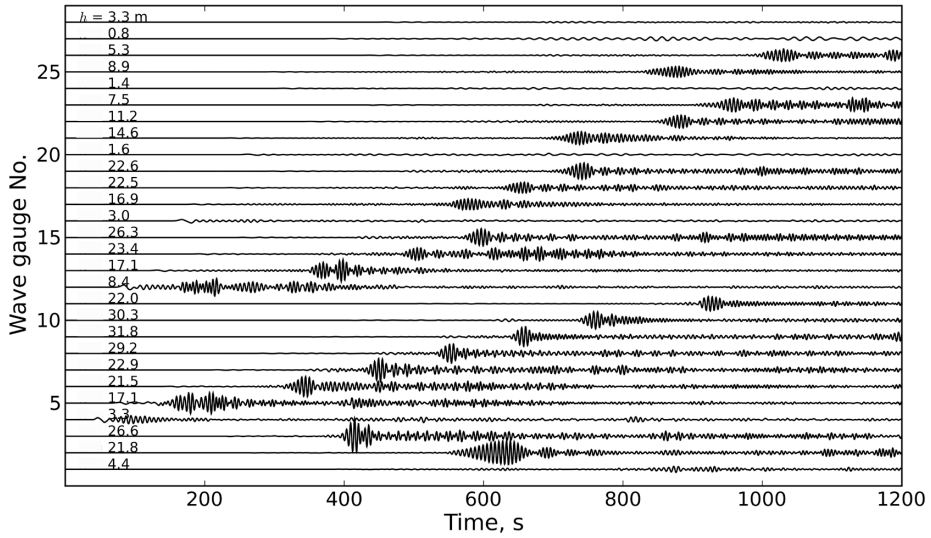

Fig. 14. Surface elevation time series at all virtual wave gauges for the outgoing leg for different water depths *h*.

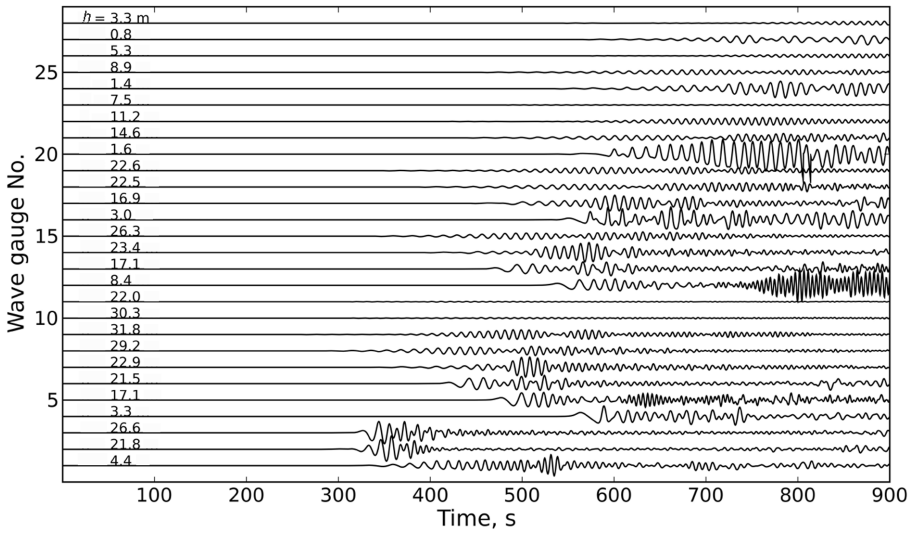

Fig. 15. Surface elevation time series at all virtual wave gauges for the ingoing leg for different water depths *h*.

Table 2. Water depth and basic wave properties at wave gauges

Wave gauge	Depth, m	Outgoing leg			Ingoing leg		
		Arrival time, s	Maximum wave amplitude, m	Wave period, s	Arrival time, s	Maximum wave amplitude, m	Wave period, s
1	4.4	873	0.18	–	531	0.66	7.3
2	21.8	639	0.74	5.4	358	0.82	9.9
3	26.6	415	1.06	5.4	344	0.69	11.2
4	3.3	94	0.24	7.0	589	0.64	14.7
5	17.1	207	0.62	5.1	524	0.46	9.6
6	21.5	345	0.60	5.4	524	0.51	8.9
7	22.9	450	0.69	5.4	508	0.62	8.6
8	29.2	557	0.57	5.4	550	0.28	8.0
9	31.8	660	0.61	5.7	490	0.29	8.9
10	30.3	758	0.52	5.7	819	0.04	–
11	22.0	922	0.44	5.7	843	0.02	–
12	8.4	217	0.52	5.7	802	0.96	4.8
13	17.1	398	0.66	5.1	566	0.43	10.9
14	23.4	678	0.41	4.8	573	0.61	8.9
15	26.3	597	0.54	5.4	631	0.26	8.3
16	3.0	167	0.08	–	662	0.78	11.2
17	16.9	578	0.34	5.4	601	0.49	9.9
18	22.5	659	0.34	5.1	807	0.30	6.1
19	22.6	744	0.51	5.4	682	0.22	8.3
20	1.6	693	0.08	–	801	0.90	8.6
21	14.6	740	0.39	5.4	893	0.29	7.7
22	11.2	883	0.39	5.7	762	0.23	8.0
23	7.5	1129	0.43	5.1	753	0.04	–
24	1.4	1093	0.08	–	781	0.45	10.9
25	8.9	881	0.32	5.4	862	0.16	–
26	5.3	1030	0.38	5.7	867	0.11	–
27	0.8	856	0.11	–	869	0.23	13.7
28	3.3	1117	0.03	–	885	0.11	–

Kiirlaevalainete mustrist Tallinna lahel

Tomas Torsvik ja Tarmo Soomere

On analüüsitud kiirlaevalainete ruumilist mustrit Tallinna lahel Boussinesqi võrranditel baseeruva lainemudeli COULWAVE abil. Aluseks on võetud 7.10.2007 salvestatud laeva SuperSeaCat trajektoor ja kiirus. Laevalainete kõrgus laevatee lähistel varieerub mitmekordselt, sõltuvalt laeva kiirusest ja konkreetsest merealast. Enamasti on lainekõrgus alla 1 m. Kõrgeimad lained tekivad siis, kui laev sõidab Tallinna sadamale lähenedes transkriitilises režiimis. Selles režiimis tekkinud lainete kõrgus on kuni 3 m. Need mõjutavad enim Pirita randa, kus kiirlaevalainete osakaal võib olla märksa suurem kui Viimsi poolsaare muudes osades.